Journal of The Electrochemical Society, **156** (5) B572-B579 (2009)
0013-4651/2009/156(5)/B572/8/$23.00 © The Electrochemical Society

Phase Relationship of CsH_2PO_4–$CsPO_3$ System and Electrical Properties of $CsPO_3$

Yu-ki Taninouchi,[z] Naoyuki Hatada, Tetsuya Uda,[*] and Yasuhiro Awakura

Department of Materials Science and Engineering, Kyoto University, Sakyo, Kyoto 606-8501, Japan

The dehydration behavior of the paraelectric phase of CsH_2PO_4 was investigated by thermogravimetric and X-ray diffraction analyses, and then the phase diagrams of CsH_2PO_4–$CsPO_3$ system were established. The relationship between the onset temperature of dehydration (T_{dehy}/K) and the partial pressure of water (p_{H_2O}/atm) is $\log p_{H_2O} = 7.62(\pm 1.18) - 4.42(\pm 0.56)(1000/T_{dehy})$ below 228°C. The thermodynamically stable phase just above T_{dehy} is the fully dehydrated product $CsPO_3(s)$, although partially dehydrated products transiently appeared in the course of the dehydration to $CsPO_3$. Such developments allowed us to complete the temperature-humidity phase diagram and to regard the composition-temperature phase diagram as the eutectic type. This paper also reports the phase transition and electrical properties of $CsPO_3$ examined by differential thermal analysis, ac impedance spectroscopy, and dc polarization measurement. The just-synthesized $CsPO_3$ showed the relatively high electrical conductivity in unhumidified Ar. Ionic conductivity as high as 5×10^{-4} S cm^{-1} was observed on heating from 150 to 450°C. Such high ionic conductivity disappeared after first heating up to 620°C and was explained by the proton diffusion through the absorbed H_2O. At around 600°C, a high-temperature phase of $CsPO_3$ showed the electrical conductivity as high as 10^{-3} S cm^{-1}. However, this conductivity was not purely ionic.
 [DOI: 10.1149/1.3086755]

Manuscript submitted September 23, 2008; revised manuscript received January 26, 2009. Published March 5, 2009.

Cesium dihydrogen phosphate (CsH_2PO_4) in the group of solid acids undergoes a transition from a paraelectric phase to a superprotonic phase at 228°C.[1-5] At the phase transition, the proton conductivity increases by three orders of magnitude and exceeds 10^{-2} S cm^{-1}. The stable operation of CsH_2PO_4 as a fuel cell electrolyte was demonstrated by Boysen et al.[6] and by Otomo et al..[7] Recently, fabrication routes to obtain high powder density[8] and utilization of alcohol fuel[9] have been reported. CsH_2PO_4, therefore, has received attention as a promising solid electrolyte for intermediate-temperature fuel cells in the temperature range from 200 to 300°C. However, this compound has a challenge in phase stability. Under insufficient humidified conditions, CsH_2PO_4 starts dehydration/decomposition with polymerization of phosphate anions as follows

$$CsH_2PO_4(s) \rightarrow CsH_{2(1-x)}PO_{4-x}(s \text{ or } l) + xH_2O(g) \qquad 0 < x \leqslant 1 \qquad [1]$$

Thus, it is important for practical applications to clarify the dehydration behavior of CsH_2PO_4.

Previously, we reported the detailed dehydration behavior from the superprotonic phase of CsH_2PO_4 [$CsH_2PO_4(s,\text{sp})$, sp: superprotonic phase] that is obtained above ca. 228°C.[10] The relationship between the onset temperature of dehydration (T_{dehy}) and the partial pressure of water (p_{H_2O}) was determined. In the temperature range from 228 to ca 260°C, $CsH_2PO_4(s,\text{sp})$ fully dehydrates to solid cesium metaphospahte [$CsPO_3(s)$, $x = 1$ in Eq. 1] accompanying the formation of partially dehydrated product of solid cesium hydrogen pyrophosphate [$CsHPO_{3.5}(s)$, $x = 0.5$ in Eq. 1, $CsHPO_{3.5}$ is often expressed as $Cs_2H_2P_2O_7$] as a transient phase. Above ca. 260°C,[11] $CsH_2PO_4(s,\text{sp})$ first dehydrates to stable phase of liquid [$CsH_{2(1-\delta)}PO_{4-\delta}(l)$], where the fraction of dehydration (δ) is about 0.4; the value, however, varies depending on the humidity and temperature. The liquid phase finally dehydrates to $CsPO_3(s)$.

In this study, for a comprehensive understanding of the dehydration behavior of CsH_2PO_4, we investigate the dehydration reaction from the paraelectric phase of CsH_2PO_4 [$CsH_2PO_4(s,\text{pe})$, pe: paraelectric phase] at temperatures lower than 228°C. On the basis of the results of this study as well as those in previous reports,[10,11] the temperature-humidity phase diagram of CsH_2PO_4 is completed and a composition-temperature phase diagram of CsH_2PO_4–$CsPO_3$ system is developed. These phase diagrams are useful for researchers developing CsH_2PO_4-type fuel cells. As far as we know, there is no report about the electrical properties of $CsPO_3$, which is the final dehydration product. The just synthesized $CsPO_3$ showed relatively high electrical conductivity. Thus, the thermal and electrical properties of $CsPO_3$ are also investigated in detail.

Experimental

Dehydration behavior of CsH_2PO_4.— Polycrystalline powder of CsH_2PO_4 was prepared from $CsCO_3$–H_3PO_4 aqueous solutions by the introduction of methanol.[4,12] X-ray powder diffraction (XRD) was utilized to confirm that the desired phase had been obtained.[13] In addition, the ratios of phosphorus (P) and cesium (Cs) in the powder were checked using inductively coupled plasma atomic emission spectrometry and an atomic adsorption spectrophotometer, respectively.

A thermogravimetric (TG) analysis (TGA) of CsH_2PO_4 powder was carried out using a Rigaku TG-DTA/HUM with the platinum sample container. The weight of the sample was ~25 mg. p_{H_2O} around the sample was controlled by flowing humidified Ar-gas at the rate of ~400 mL min^{-1}.

Phase identification was carried out via XRD analysis on a Rigaku 2200 using Cu Kα radiation. The diffraction pattern of the sample at various levels of dehydration was collected at room temperature.

Thermal and electrical properties of $CsPO_3$.— Polycrystalline powder of $CsPO_3$, which is the final dehydration product, was prepared by the dehydration reaction from CsH_2PO_4 polycrystalline powder. CsH_2PO_4 powder in a silica glass crucible was kept at 190°C for 62 h in Ar or at 220°C for 72 h in air. In each case, the final weight change was $-7.7 \pm 0.2\%$, which is evidence of the formation of $CsPO_3$ because the theoretical weight change for the dehydration reaction from CsH_2PO_4 to $CsPO_3$ is -7.84%.

A differential thermal analysis (DTA) of $CsPO_3$ powder was carried out using a Rigaku TG-DTA/HUM utilizing platinum as the reference. The sample in a platinum container was heated and cooled at the rate of 5 K min^{-1} from 200 to 800°C. Ar-gas with $p_{H_2O} = 0.0085$ atm was flowed at the rate of ~400 mL min^{-1}.

The electrical conductivity of $CsPO_3$ was examined by ac impedance spectroscopy and dc polarization measurement. The details of the experimental apparatus were shown previously.[10] For the electrical measurements, $CsPO_3$ powder was pressed uniaxially at 3 ton cm^{-2} for 10 min to form the pellets (diameter 1.11 cm, thick-

* Electrochemical Society Active Member.
[z] E-mail: taninouchi@t01.mbox.media.kyoto-u.ac.jp

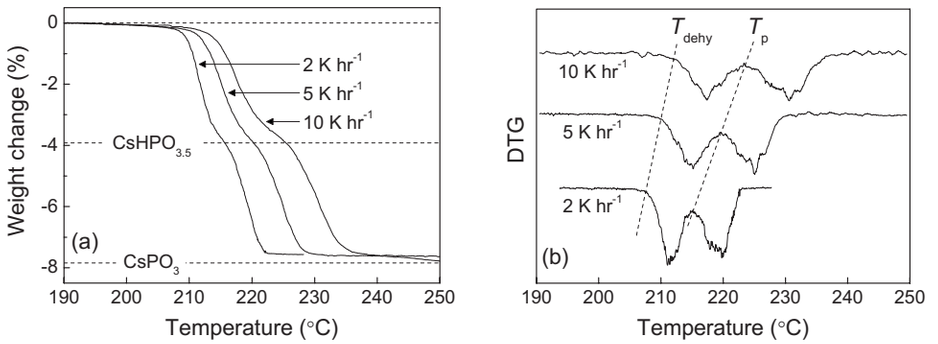

Figure 1. TGA of CsH_2PO_4 powder at three heating rates of 2, 5, and 10 K h^{-1} under $p_{H_2O} = 0.022 \pm 0.009$ atm. (a) Temperature dependence of weight change (TG curve). Dotted lines indicate the theoretical weight changes to form $CsHPO_{3.5}$ and $CsPO_3$. (b) Differential values of weight change (DTG curve).

ness ~1 mm). Prior to forming pellets, $CsPO_3$ powder was heated at 550°C for 12 h in air to minimize the effect of absorbed H_2O and to eliminate the possibility of partial rehydration of $CsPO_3$. Silver electrodes were attached on both sides of the pellet with silver paint (Fujikura Kasei, D-550). The temperature dependence of conductivity was measured by ac impedance spectroscopy using a Solartron 1260 in the frequency range from 1 to 1 M Hz with voltage amplitude of 500 mV. The $CsPO_3$ pellet was heated and cooled at 1 K min^{-1} in the temperature range from 150 to 620°C. The measurements were performed under flowing unhumidified Ar gas. Collected impedance data were analyzed using the commercial software package Z-View. The dc polarization measurement was performed using a Solartron 1278 potentiostat. DC voltage was applied under flowing unhumidified Ar gas.

Results

Dehydration behavior of CsH_2PO_4.— TGA of CsH_2PO_4.— Figure 1 shows the results of weight change on heating at the three different rates of 2, 5, and 10 K h^{-1} under $p_{H_2O} = 0.022 \pm 0.009$ atm. Figure 1a and b shows the weight change against temperature (TG curve) and the differential values of weight change [differential TG (DTG) curve], respectively. The theoretical weight changes to form $CsPO_3$ (−7.84%) and $CsHPO_{3.5}$ (−3.92%) are also plotted as dotted lines in Fig. 1a. The TG and DTG curves revealed an onset temperature of dehydration of CsH_2PO_4 (T_{dehy} in Fig. 1), a local minimum of weight loss (T_p in Fig. 1), and subsequent completion of the reaction. A similar profile was observed in the dehydration from $CsH_2PO_4(s,sp)$, where the dehydration temperature is in the range from 228 to 260°C.[10]

The phase-boundary between $CsH_2PO_4(s,pe)$ and dehydration product was determined by the value of T_{dehy}. T_{dehy} in Fig. 1 is an apparent value because it increases with a rise in heating rate. True T_{dehy} was estimated by the extrapolation against the square root of heating rate.[10] Figure 2a shows the extrapolation of the apparent T_{dehy} under $p_{H_2O} = 0.022 \pm 0.009$ atm to zero heating rate. This extrapolation is reasonable because a linear relationship can clearly be seen. Similar measurements were repeated under four different p_{H_2O}. The results are summarized in the Arrhenius form in Fig. 2b. A good linear relationship between the inverse temperature and $\log(p_{H_2O})$ is evident by the dotted line. The resultant relationship between p_{H_2O}(atm) and T_{dehy}(K) is described by

$$\log p_{H_2O} = 7.62(\pm 1.18) - 4.42(\pm 0.56)\frac{1000}{T_{dehy}} \qquad [2]$$

The total weight loss at the end of the reaction as seen in Fig. 1a was in excellent agreement with the theoretical weight loss to form $CsPO_3$ for all heating rates. The sample after TGA remained in the form of loose powder. Thus, the dehydration from $CsH_2PO_4(s,pe)$ to $CsPO_3(s)$ was not through the liquid phase.

Figure 3 shows the results of isothermal TGA. Figure 3a and b are TG/DTG curves at 190°C under $p_{H_2O} = 0.0085 \pm 0.0003$ atm and at 218°C under $p_{H_2O} = 0.0354 \pm 0.0015$ atm, respectively. These temperatures are slightly higher than the equilibrium T_{dehy} implied by Eq. 2. That is, with the given p_{H_2O}, CsH_2PO_4 should dehydrate at 183 ± 3 and 214 ± 3°C, respectively. In either condition, final weight losses were in excellent agreement with the theo-

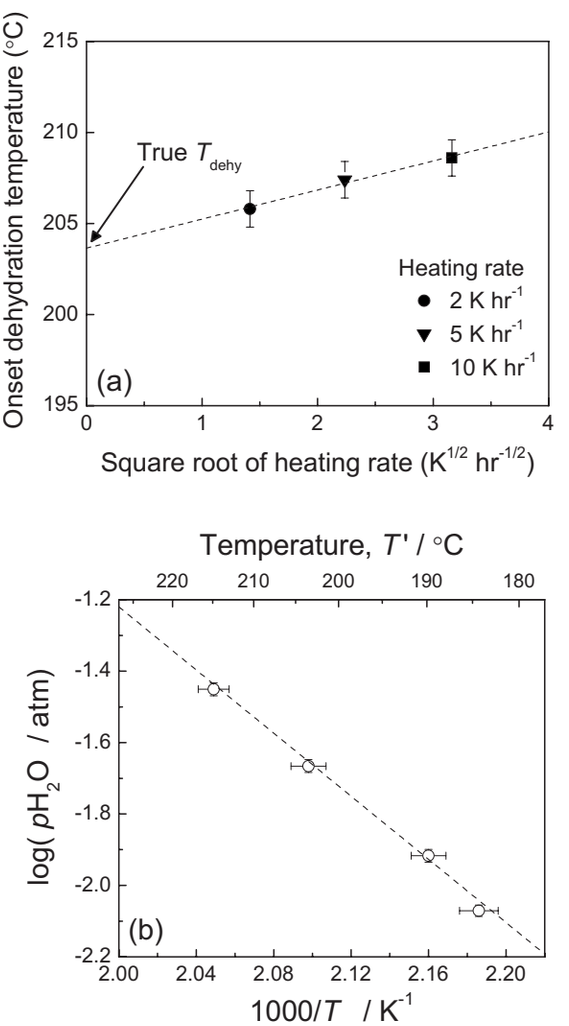

Figure 2. (a) Extrapolation of the onset temperatures of dehydration (T_{dehy}) under $p_{H_2O} = 0.022 \pm 0.009$ atm to the heating rate of zero. Apparent T_{dehy} is assumed to be proportional to the square root of the heating rate. (b) Summary of true T_{dehy} under various p_{H_2O}. A linear relationship existed in Arrhenius form.

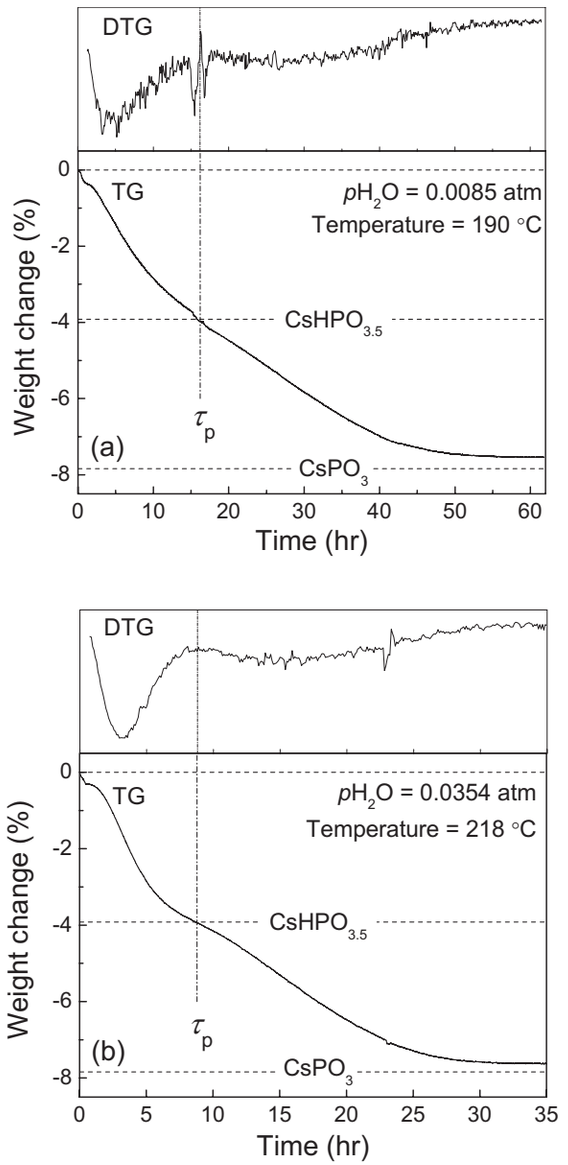

Figure 3. TGA of CsH_2PO_4 powder at the constant temperature of (a) 190°C under p_{H_2O} = 0.0085 ± 0.0003 atm and (b) 218°C under p_{H_2O} = 0.0354 ± 0.0015 atm.

retical value to form the fully dehydrated product of $CsPO_3$. Partially dehydrated products, such as $CsHPO_{3.5}$, could not be obtained as a stable phase. However, a local minimum of weight loss appeared at a time of τ_p in Fig. 3, where the weight loss almost coincided with the theoretical value to form $CsHPO_{3.5}$.

X-ray diffraction analysis of dehydration products.— Figure 4 shows the XRD patterns of samples at various levels of dehydration. The diffraction pattern of nondehydrated $CsH_2PO_4(s,pe)$ is shown in Fig. 4a, which agreed with the diffraction pattern for paraelectric phase of CsH_2PO_4 provided in the JCPDS database,[13] and the impurity phases were not seen. The diffraction pattern of fully dehydrated $CsPO_3(s)$ is shown in Fig. 4d. Fully dehydrated $CsPO_3$ was prepared by heating $CsH_2PO_4(s,pe)$ at 215°C for 94 h under unhumidified Ar gas. The weight change of −7.9% agreed with the theoretical weight change to form $CsPO_3$ (−7.84%). In addition, the pattern in Fig. 4d was in excellent agreement with the diffraction pattern for $CsPO_3$, which we reported previously.[10] Meanwhile, Fig.

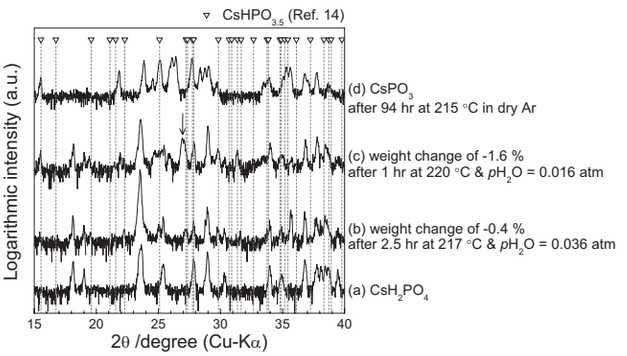

Figure 4. XRD patterns of samples at the various extent of dehydration. The diffraction patterns were collected at room temperature. The positions of diffraction peaks from $CsHPO_{3.5}$ are also shown.[14] (a) Nondehydrated CsH_2PO_4. (b) Partially dehydrated sample. $CsH_2PO_4(s,pe)$ was kept for 2.5 h at 217°C and p_{H_2O} = 0.036 atm. Fixed temperature was 3 ± 3°C higher than T_{dehy}. Weight change was −0.4%. (c) Partially dehydrated sample. $CsH_2PO_4(s,pe)$ was kept for 1 h at 220°C in air (p_{H_2O} = about 0.016 atm). Fixed temperature was ~25°C higher than T_{dehy}. Weight change was −1.6%. Arrowed line indicates typical peak of unknown phase. (d) Fully dehydrated $CsPO_3$, which was prepared by keeping $CsH_2PO_4(s,pe)$ at 215°C for 94 h in unhumidified Ar.

4b and c show the diffraction pattern of the partially dehydrated sample where weight changes are −0.4 and −1.6%, respectively. In Fig. 4b, $CsH_2PO_4(s,pe)$ was kept for 2.5 h at 217°C and p_{H_2O} = 0.036 atm, where the temperature was 3 ± 3°C higher than T_{dehy} in Eq. 2. In Fig. 4c, $CsH_2PO_4(s,pe)$ was kept for 1 h at 220°C in air (p_{H_2O} = about 0.016 atm), where the temperature was ~25°C higher than T_{dehy} in Eq. 2. This means the latter condition was a shorter time but had a larger driving force for the dehydration reaction than the former condition. The positions of diffraction peaks of $CsHPO_{3.5}$ reported in the JCPDS database[14] are also shown in Fig. 4. The pattern in Fig. 4b could be explained by the mixture of CsH_2PO_4 and $CsHPO_{3.5}$. In the pattern in Fig. 4c, unknown peaks (a typical one is indicated by an arrowed line) were observed along with the peaks of CsH_2PO_4, $CsHPO_{3.5}$, and $CsPO_3$.

Thermal and electrical properties of $CsPO_3$.— *DTA of $CsPO_3$.*— Figure 5 shows the DTA profile of $CsPO_3$ powder at the heating/cooling rate of 5 K min^{-1}. Two endothermic peaks and two exothermic peaks were seen on heating and cooling, respectively.

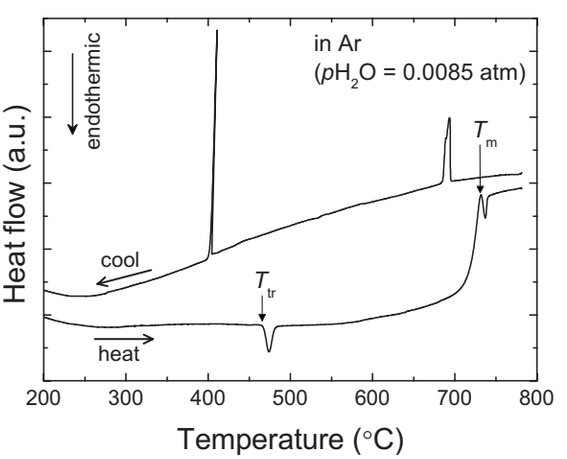

Figure 5. DTA of $CsPO_3$ powder at the heating/cooling rate of 5 K min^{-1} under p_{H_2O} = 0.0085 ± 0.0003 atm. T_{tr} and T_m mean the transition temperature to the high-temperature phase and melting point of $CsPO_3$, respectively.

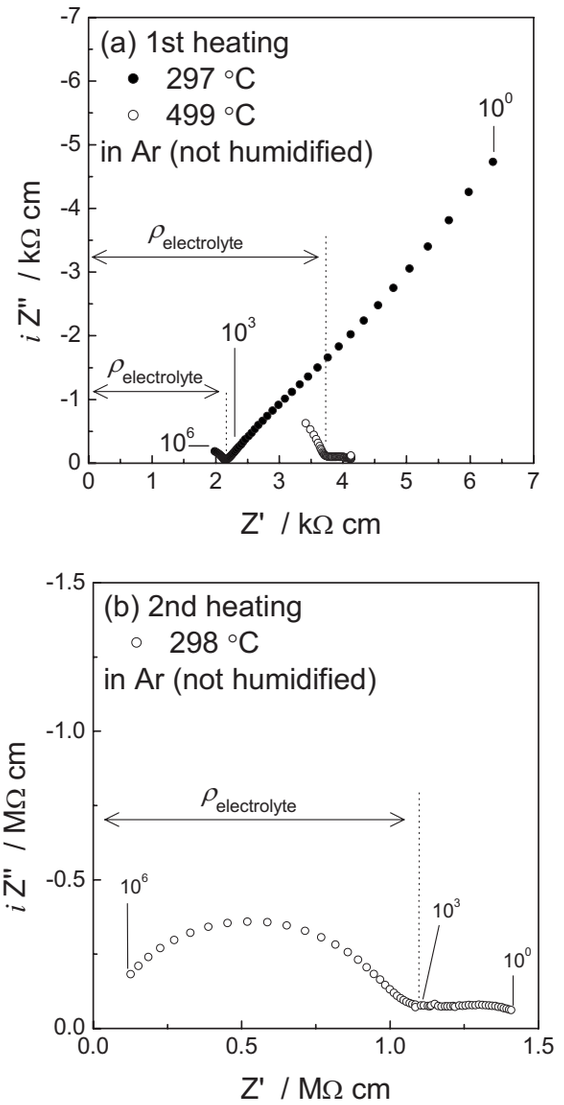

Figure 6. Typical impedance spectra of $CsPO_3$. (a) At 297 and 499°C on first heating and (b) at 298°C on second heating.

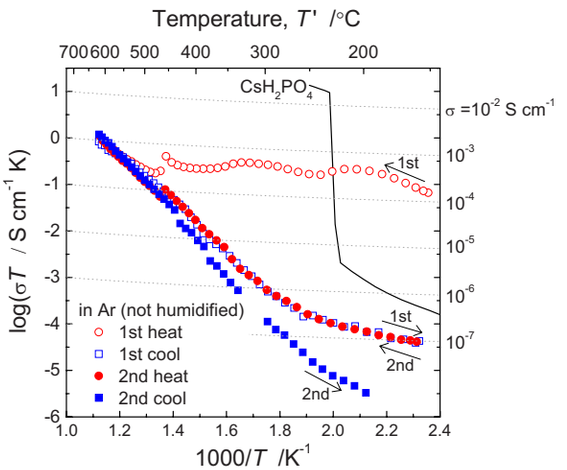

Figure 7. (Color online) Temperature dependence of electrical conductivity of $CsPO_3$ in unhumidified Ar. $CsPO_3$ pellet was heated and cooled at the rate of 1 K min^{-1}. The results of two heating and cooling cycles are presented. Conductivity change of CsH_2PO_4 on heating under p_{H_2O} = 0.3 atm is also plotted as a solid line.

The sample shape after DTA suggested melting in the course of the temperature sweep. Onset temperatures of two endothermic peaks on heating were 467°C (T_{tr} in Fig. 5) and 733°C (T_m in Fig. 5), respectively. It was reported that $CsPO_3$ exhibits a phase transition to high temperature phase at ~480°C and melts at ~735°C.[15,16] Thus, the endothermic and exothermic peaks at the higher temperature side around 700°C indicate the melting and freezing of $CsPO_3$ [$CsPO_3(s) \leftrightarrow CsPO_3(l)$], respectively. The endothermic peak at T_{tr} in Fig. 5 indicates the phase transition from the low to high-temperature phase of solid $CsPO_3$ [$CsPO_3(s) \rightarrow CsPO_3(s,ht)$, ht: high temperature phase]. It is also noteworthy that the XRD pattern of the $CsPO_3$ furnace cooled from liquid at 800°C using a muffle furnace was in good agreement with the diffraction pattern of $CsPO_3$ before DTA (pattern not shown). Thus, the phase of $CsPO_3$ after DTA should be the same as that before DTA, and the exothermic peak at ~400°C on cooling corresponds to the phase transition from $CsPO_3(s,ht)$ to $CsPO_3(s)$. The phase transition between $CsPO_3(s)$ and $CsPO_3(s,ht)$ was reversible but showed large thermal hysteresis of ~60°C.

AC impedance spectroscopy of $CsPO_3$.— Figure 6 shows typical impedance spectra of $CsPO_3$ obtained (a) at 297 and 499°C on first heating and (b) at 298°C on second heating. The measurements were performed in unhumidified Ar. At 297°C on first heating (Fig. 6a), one arc and one almost straight line were seen in higher and lower frequency regions, respectively. The resistivity of $CsPO_3$ electrolyte ($\rho_{electrolyte}$) was evaluated by the intersection between the arc and the real axes, as indicated in Fig. 6a. The straight line can be explained by the polarization phenomena at the electrolyte/electrode interfaces. Large polarization at the interfaces with Ag electrodes suggests that ionic conduction exists in $CsPO_3$. At 499°C on first heating (Fig. 6a), where $CsPO_3$ shows high-temperature phase, one arc and deviated semicircle were seen in the higher and lower frequency regions, respectively. The resistivity of $CsPO_3$ was evaluated by the intersection between the arc at higher frequency and the real axes, as indicated in Fig. 6a. The semicircle at the lower frequency region was probably attributed by the electrolyte/electrode interfaces. Meanwhile, the impedance spectrum collected at 298°C on second heating showed two distinct semicircles. It was estimated that the clear semicircle at the higher frequency region and the deviated semicircle at the lower frequency region corresponded to the $CsPO_3$ electrolyte and the electrolyte/electrode interfaces, respectively.

Figure 7 shows the conductivity of $CsPO_3$ as a function of temperature for two heating/cooling cycles. The conductivity of CsH_2PO_4 is also represented as a solid line. On first heating, $CsPO_3$ showed the relatively high conductivity of about 5×10^{-4} S cm^{-1} at the intermediate temperature from 150 to 450°C. However, this high conductivity at the intermediate temperature disappeared after first heating. The conductivity at 300°C on first cooling and second heating was about three orders of magnitude lower than the value on first heating. Furthermore, the conductivity at 300°C on second cooling was about four orders of magnitude lower than the value on first heating. At ~600°C, $CsPO_3$ in the high-temperature phase exhibited conductivity as high as 10^{-3} S cm^{-1} in any heating/cooling cycle. It is also noteworthy that the conductivity jumps at the transition temperature [$CsPO_3(s) \leftrightarrow CsPO_3(s,ht)$, at 467°C on heating] were not large, even though an abrupt small change of conductivity existed at the phase transition on heating.

DC polarization measurement of $CsPO_3$.— DC polarization measurements were performed at two different temperatures in Ar (not humidified). Figure 8 shows the change of current with time and the relationship between steady current and voltage at 250 ± 2°C and at 543 ± 2°C. Prior to the measurements, $CsPO_3$ pellets were not treated at high temperature. Thus, the experimental conditions of dc

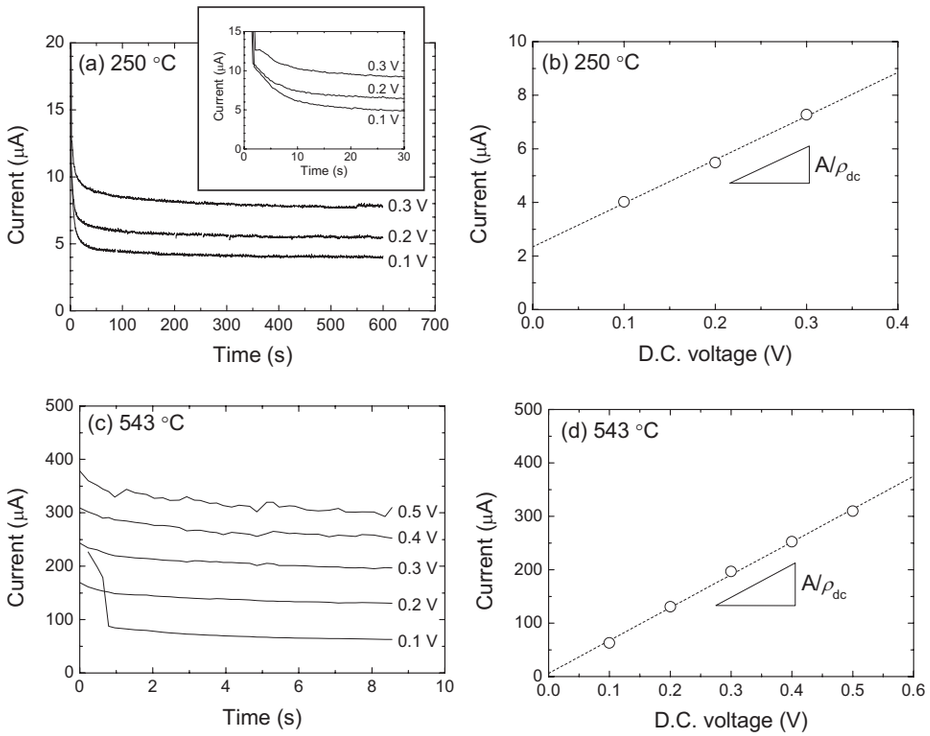

Figure 8. Results of dc polarization measurements. (a) Change of current at 250 ± 2°C with time. (b) Current in steady state as a function of dc voltage at 250 ± 2°C. (c) Change of dc current at 543 ± 2°C with time. (d) Current in steady state as a function of dc voltage at 543 ± 2°C. Constant "A" in (b) and (d) refers to the geometry factors of $CsPO_3$ pellets.

polarization measurements correspond to those of first heating of conductivity measurement, as Fig. 7 shows. At 250°C, dc voltages of 0.1, 0.2, and 0.3 V were each applied for 600 s. DC current rapidly decreased with time, as seen in Fig. 8a. The dc current at 600 s is plotted as a function of applied dc voltage in Fig. 8b. An obvious linear relationship was obtained (shown as the dotted line). The resistivity when applying the dc voltage, ρ_{dc}, was evaluated from the slope of the dotted line in Fig. 8b. In Table I, ρ_{dc} is summarized with the resistivity of $CsPO_3$ ($\rho_{electrolyte}$) evaluated by ac impedance spectroscopy in the same conditions. At 250°C, ρ_{dc} (4.18×10^5 Ω cm) was 2 orders of magnitude higher than $\rho_{electrolyte}$ (3.89×10^3 Ω cm).

Meanwhile, at 543°C, dc voltages of 0.1, 0.2, 0.3, 0.4, and 0.5 V were each applied for 8.5 s. At this temperature, $CsPO_3$ showed the high-temperature phase. Compared to the current change with time at 250°C in Fig. 8a, the reduction rate of dc current was small at 543°C, as seen in Fig. 8c. ρ_{dc} was evaluated based on the dc currents at 8.5 s, as shown in Fig. 8d. ρ_{dc} and $\rho_{electrolyte}$ at 543°C are also summarized in Table I. At 543°C, ρ_{dc} (1.10×10^4 Ω cm) did not show a large difference from $\rho_{electrolyte}$ (6.59×10^3 Ω cm) and was about half the time of $\rho_{electrolyte}$.

Table I. Resistivity evaluated by dc polarization measurement (ρ_{dc}) and ac impedance spectroscopy ($\rho_{electrolyte}$), and calculated transference numbers for ion conduction (TN_i) and electron/hole conduction (TN_e).

Temperature (°C)	ρ_{dc} (Ω cm)	$\rho_{electrolyte}$ (Ω cm)	TN_i	TN_e
250 ± 2	$4.18 (\pm 0.26) \times 10^5$	3.89×10^3	0.99	0.01
543 ± 2[a]	$1.10 (\pm 0.03) \times 10^4$	6.59×10^3	0.40	0.60

[a] $CsPO_3$ exhibits the high-temperature phase [$CsPO_3(s,ht)$].

Discussion

Mechanism of dehydration reaction.— The weight change at iso-temperatures in Fig. 3 indicated that the stable dehydration phase just above T_{dehy} is $CsPO_3(s)$. However, $CsHPO_{3.5}(s)$ appeared as a transient phase in the course of dehydration as seen in the XRD analysis. This situation is the same as we found in our experiments of dehydration in the temperature range from 228 to 260°C.[10] The existence of a transient phase complicates the thermodynamic analysis and reaction mechanism. There are two possibilities for the thermodynamic meaning of the T_{dehy} in Eq. 2: onset temperature of the dehydration from CsH_2PO_4 to $CsHPO_{3.5}$ and that from CsH_2PO_4 to $CsPO_3$. Considering each equilibrium (or quasi equilibrium) at a given temperature, p_{H_2O} can be written as

$$2CsH_2PO_4(s,pe) = 2CsHPO_{3.5}(s) + H_2O(g) \qquad [3]$$

$$\ln p^{(3)}_{H_2O} = \frac{-\Delta_{dehy}G^{\circ}_{(3)}(T)}{RT}$$

$$CsH_2PO_4(s,pe) = CsPO_3(s) + H_2O(g) \qquad [4]$$

$$\ln p^{(4)}_{H_2O} = \frac{-\Delta_{dehy}G^{\circ}_{(4)}(T)}{RT}$$

where $\Delta_{dehy}G^{\circ}_{(i)}$ is the standard Gibbs energy of the dehydration reactions of Eq. 3 and 4 at Kelvin temperature T, R is the gas constant, and $p^{(i)}_{H_2O}$ is the partial pressure of water in equilibrium Eq. 3 or 4. It is assumed that we take pure substances as standard state, and the reactant CsH_2PO_4 and the products $CsHPO_{3.5}$ and $CsPO_3$ do not have mutual solubility. In Eq. 3, quasi-equilibrium is established between CsH_2PO_4 and $CsHPO_{3.5}$.

Because $CsPO_3$ is a thermodynamically stable phase just above T_{dehy}, the mixture of CsH_2PO_4 and $CsPO_3$ is more stable than $CsHPO_{3.5}$

$$2CsHPO_{3.5}(s) \rightarrow CsH_2PO_4(s,pe) + CsPO_3(s) \quad \Delta G^{\circ}_{(5)}(T) < 0 \quad [5]$$

Therefore

$$\ln p^{(3)}_{H_2O} - \ln p^{(4)}_{H_2O} = \frac{-[\Delta_{dehy}G^{\circ}_{(3)}(T) - \Delta_{dehy}G^{\circ}_{(4)}(T)]}{RT} = \frac{\Delta G^{\circ}_{(5)}(T)}{RT} < 0 \quad [6]$$

Equation 6 means that, at a fixed temperature, the p_{H_2O} quasi-equilibrating CsH_2PO_4 with $CsHPO_{3.5}$ is lower than that equilibrating CsH_2PO_4 with $CsPO_3$. Furthermore, at a given p_{H_2O}, the following relationships exist

$$T^{(7)} = \frac{-\Delta_{dehy}G^{\circ}_{(3)}[T^{(7)}]}{R \ln p_{H_2O}} \quad [7]$$

$$T^{(8)} = \frac{-\Delta_{dehy}G^{\circ}_{(4)}[T^{(8)}]}{R \ln p_{H_2O}} \quad [8]$$

$$\Delta_{dehy}G^{\circ}_{(3)}[T^{(8)}] - \Delta_{dehy}G^{\circ}_{(3)}[T^{(7)}] = -[T^{(8)} - T^{(7)}]\Delta_{dehy}S^{\circ}_{(3)} \quad [9]$$

where it is reasonable to assume that the standard enthalpy change, $\Delta_{dehy}H^{\circ}$, and the standard entropy change, $\Delta_{dehy}S^{\circ}$, for Reactions 3 and 4 are constant in the considered temperature range. Subtracting Eq. 8 from Eq. 7, we obtain

$$T^{(7)} - T^{(8)} = -\frac{\Delta_{dehy}G^{\circ}_{(3)}[T^{(7)}] - \Delta_{dehy}G^{\circ}_{(4)}[T^{(8)}]}{R \ln p_{H_2O}} \quad [10]$$

Then, we substitute Eq. 9 into Eq. 10 for $\Delta_{dehy}G^{\circ}_{(3)}[T^{(7)}]$ to come out. The result is

$$T^{(7)} - T^{(8)} = \frac{\Delta_{dehy}G^{\circ}_{(5)}[T^{(8)}]}{R \ln p_{H_2O} - \Delta_{dehy}S^{\circ}_{(3)}} \quad [11]$$

Now, $\Delta_{dehy}S^{\circ}_{(3)}$ is a positive value because the reaction is a gas-evolution reaction, and $R \ln p_{H_2O}$ is a negative value, which means $T^{(7)} - T^{(8)} > 0$. This implies that the dehydration reaction from CsH_2PO_4 to $CsPO_3$ occurs at lower temperature on heating than the dehydration reaction from CsH_2PO_4 to $CsHPO_{3.5}$, thermodynamically. Therefore, we can regard $T^{(8)} = T_{dehy}$ (T_{dehy} is the value determined by experiment). Meanwhile, we observed formation of $CsHPO_{3.5}$ at the initial stage even at just above T_{dehy} (+3°C), as seen in Fig. 4b. This suggests that the difference between $T^{(7)}$ and $T^{(8)}$ is very small.

As a result, the driving force of the dehydration reaction from CsH_2PO_4 to $CsPO_3$, as well as the driving force of the dehydration reaction from CsH_2PO_4 to $CsHPO_{3.5}$, are generated at a slightly higher temperature than T_{dehy}. Kinetically speaking, the rate of the dehydration reaction from CsH_2PO_4 to $CsPO_3$ should be much smaller than that from CsH_2PO_4 to $CsHPO_{3.5}$ because the former is a polymerization reaction of PO_4^{3-} anion and the latter is a reaction of dimmer formation of PO_4^{3-} anion. For this reason, $CsHPO_{3.5}$ appears as a transient phase. The transient appearance of $CsHPO_{3.5}$ probably explains the local minimum in the weight change profile (T_p in Fig. 1, τ_p in Fig. 3), where the weight loss is in good agreement with the theoretical value to form $CsHPO_{3.5}$. It is also notable that an unknown product was detected by XRD analysis in Fig. 4c when $CsH_2PO_4(s,pe)$ partially dehydrates at a much higher temperature than T_{dehy}. It is possible that the driving force to form other partially dehydrated species are generated at much higher temperature than T_{dehy}.

Table II. Standard enthalpy, entropy, and Gibbs energy of the formation of $CsPO_3$ at 298 K. Estimated values were compared to the reported values.[10,17]

	Δ_fH° (kJ mol^{-1})	Δ_fS° (J mol^{-1} K^{-1})	Δ_fG° (kJ mol^{-1})	Source
$CsPO_3$ (*s*)	−1238 (±11)	−324 (±23)	−1141 (±18)	This study
	−1242 (±9)	−330 (±17)	−1144 (±14)	Ref. 10
	−1241.4	—	—	Ref. 17

Thermodynamic evaluation for onset temperature of dehydration.— Thermodynamical properties of $CsPO_3(s)$ are re-evaluated by the relationship between T_{dehy} and p_{H_2O} in Eq. 2. The detailed evaluation procedure was shown previously.[10] We can regard T_{dehy} in Eq. 2 as $T^{(8)}$ in Eq. 8. Inserting the numeric values yields

$$\Delta_{dehy}H^{\circ} = 84.6 \pm 10.7 \text{ kJ mol}^{-1}, \quad \Delta_{dehy}S^{\circ} = 146 \pm 23 \text{ J mol}^{-1} \text{ K}^{-1} \quad [12]$$

We assume that $\Delta_{dehy}H^{\circ}$ and $\Delta_{dehy}S^{\circ}$ are constant in the temperature range to 298 K. On the basis of the standard enthalpy and entropy of formation of $CsH_2PO_4(s,pe)$ and $H_2O(g)$ at 298 K[10,17] as well as Eq. 12, thermodynamic properties of formation of $CsPO_3(s)$ can be calculated as shown in Table II. Table II also shows the values in the literature[17] and those evaluated in our previous study,[10] where the dehydration from the superprotonic phase was investigated above 228°C. The values evaluated in this study are self-consistent with previous results.

Electrical conduction in $CsPO_3$.— The final dehydration product of $CsPO_3$ showed relatively high electrical conductivity in two conditions: (*i*) at an intermediate temperature anywhere between 150 and 450°C only during first heating and (*ii*) at around 600°C, where $CsPO_3$ is in the high-temperature phase for any heating/cooling cycles. Thus, we discuss the mechanism of high electrical conduction in $CsPO_3$.

Conductivity as high as 5×10^{-4} S cm^{-1} was seen at intermediate temperatures in the range from 150 to 450°C on first heating as seen in Fig. 7. DC polarization measurement showed that ρ_{dc} was about two orders of magnitude higher than $\rho_{electrolyte}$ in ac impedance measurement. DC polarization measurement was performed in Ar (not humidified). It is a reasonable assumption that the Ag electrode provides electron, but it is quite difficult for the Ag electrode in unhumidified Ar to work for ionic species such as protons and oxide ions. That is, the Ag electrode is considered to be a blocking electrode for ionic conductors. We can regard that the current in steady state, when dc voltage is applied, is due to the current flow by electrons or holes. Thus, ρ_{dc} corresponds to the resistivity of electron/hole flow. Meanwhile, $\rho_{electrolyte}$ obtained by ac impedance spectroscopy should correspond to the resistivity of diffusion of all mobile carriers (i.e., the sum of ion, electron, and hole diffusion). As a result, the transference numbers of ions (TN_i) and sum of those of electrons and holes (TN_e) can be estimated from ρ_{dc} and $\rho_{electrolyte}$, while the estimated values are preliminary ones. The estimated transference numbers are shown in Table I. At 250°C, TN_i was 0.99 and the type of conduction of $CsPO_3$ was ionic. Although the mobile ion and its conduction mechanism are still unclear, we speculate that proton diffusion occurs through the absorbed H_2O on the surface and interface. $CsPO_3$ powder kept in a dry desiccator was pelletized at ambient temperature under atmospheric conditions. We believe that some amount of H_2O in air was absorbed during pelletizing. It is also noteworthy that it was difficult to detect further weight changes when $CsPO_3$ powder, which was dehydrated at above 200°C and, subsequently quenched, was kept at the ambient temperature under atmospheric conditions. Thus, the amount of ab-

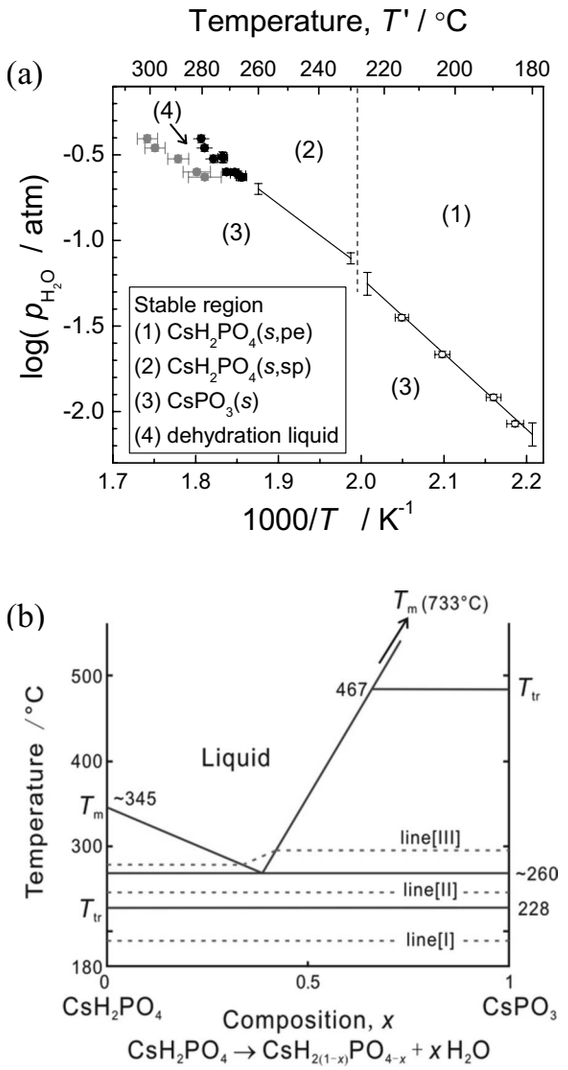

Figure 9. Phase diagrams of CsH_2PO_4 system. (a) Temperature-humidity diagram. $CsH_2PO_4(s,pe)$, $CsH_2PO_4(s,sp)$, $CsPO_3(s)$, and dehydration-liquid are thermodynamically stable in regions 1, 2, 3, and 4, respectively. (b) Preliminary composition-temperature diagram of CsH_2PO_4–$CsPO_3$ system. Lines I, II, and III mean the iso-p_{H_2O} lines of the three kinds of dehydration pathway.

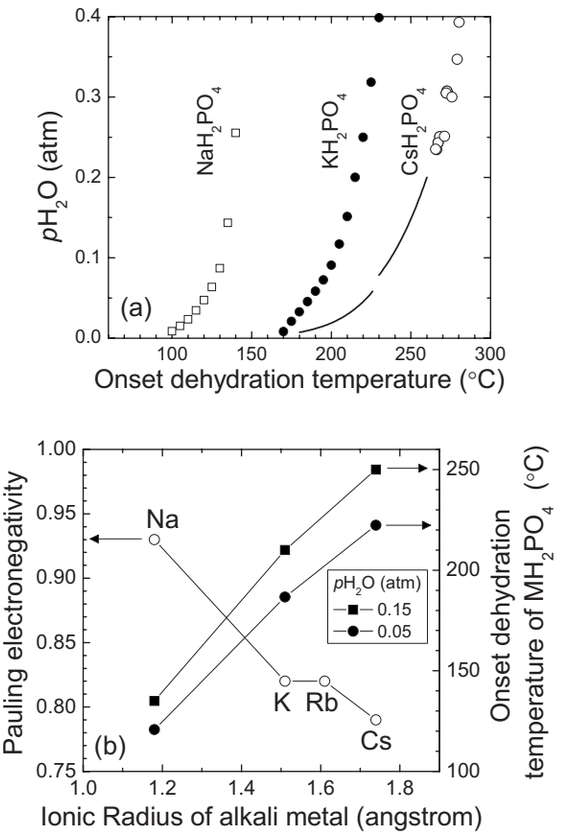

Figure 10. (a) Summary of the onset temperatures of dehydration of MH_2PO_4 (alkali metal; M = Na, K, Cs). Dehydration temperatures of NaH_2PO_4 and KH_2PO_4 were values reported by Kiehl and Wallace.[19] (b) Pauling electronegativities[20] and ionic radii of alkali metals.[21] Dehydration temperatures of MH_2PO_4 (M = Na, K, Cs) at p_{H_2O} = 0.05 and 0.15 atm are also summarized.

sorbed H_2O should be very small. The disappearance of high ionic conductivity after first heating can be explained by desorption of H_2O.

Meanwhile, at around 600°C, $CsPO_3$ exhibited high conductivity of $\sim 10^{-3}$ S cm^{-1} for all heating/cooling cycles as seen in Fig. 7. TN_i and TN_e at 543°C can be defined as 0.40 and 0.60, respectively, as listed in Table I. Thus, $CsPO_3$ was estimated to be a mixed conductor at 543°C on first heating. We speculate that residual H_2O absorbed on the $CsPO_3$ surface is the origin of ionic conduction at this temperature. When $CsPO_3$ is kept at a higher temperature than 543°C, ionic conduction probably disappears and almost pure electron/hole conduction as high as 10^{-3} S cm^{-1} is observed.

Phase diagrams of CsH_2PO_4–$CsPO_3$ system.— Upon combining the results of current and previous studies,[10,11] we established phase diagrams of the CsH_2PO_4 system. In Fig. 9a, the data are summarized in Arrhenius form. $CsH_2PO_4(s,pe)$, $CsH_2PO_4(s,sp)$, $CsPO_3(s)$, and dehydration-liquid $[CsH_{2(1-\delta)}PO_{4-\delta}(l)$, δ is $\sim 0.4]$ are thermodynamically stable in regions 1, 2, 3, and 4, respectively. In the previous study, phase boundaries were determined based on the conductivity and weight changes on heating. In this diagram, we can see that CsH_2PO_4 electrolyte in a practical application must be kept in regions 1 and 2. Meanwhile, Fig. 9b shows the preliminary composition-temperature phase diagram of the CsH_2PO_4–$CsPO_3$ system estimated based on Fig. 9a. The melting point of CsH_2PO_4 can be estimated at $\sim$345°C based on the data reported by Rapoport et al.[18] $CsPO_3$ exhibits phase transition to high-temperature phase at 467°C and melts at 733°C, as seen in Fig. 5. $CsHPO_{3.5}$ is not a stable phase and CsH_2PO_4 dehydrates to liquid phase above $\sim$260°C. Thus, the CsH_2PO_4–$CsPO_3$ system is of the eutectic type without any intermediate compound of solid. Three distinct dotted lines in Fig. 9b indicate the iso-p_{H_2O} line. Each line explains the three types of dehydration pathway depending on humidity and temperature. Lines I and II are the dehydration pathways from $CsH_2PO_4(s,pe)$ to $CsPO_3(s)$, and from $CsH_2PO_4(s,sp)$ to $CsPO_3(s)$, respectively. Line III is the dehydration pathway from $CsH_2PO_4(s,sp)$ to $CsPO_3(s)$ through liquid phase.

The onset temperatures of dehydration of various alkali metal dihydrogen phosphates (MH_2PO_4, M = Na, K, Cs) are compared in Fig. 10a. Kiehl and Wallace[19] reported the values for NaH_2PO_4 and KH_2PO_4. Figure 10b shows the Pauling electronegativity of alkali metal[20] against the Shannon ionic radius.[21] Dehydration temperatures of MH_2PO_4 at p_{H_2O} = 0.05 and 0.15 atm are also shown in Fig. 10b. It is clear that stability against dehydration is improved on the order of Cs > K > Na. This trend of stability correlates inversely with the electronegativity, Cs < K < Na. Qualitatively con-

sidering solid acids, which have a strong ionic nature, a cation with smaller electronegativity makes the net charge of oxygen negatively larger. As a result, the binding of proton and oxide ion (O···H–O) between phosphate anions probably becomes stronger, which increases the dehydration temperature. Meanwhile, Boysen reported that ion size plays a key role in the appearance of superprotonic transition.[12] Superprotonic phases exist in RbH_2PO_4 and CsH_2PO_4, which have larger ratios of cation and oxy-anion, but are absent in NaH_2PO_4 and KH_2PO_4, which have smaller ratios of cation and oxy-anion. These two kinds of empirical knowledge will become a hint to find new solid acids, which have higher chemical stability against dehydration while keeping their appearance of superprotonic phase.

Conclusion

At temperatures lower than 228°C, the relationship between the onset temperature of dehydration (T_{dehy}/K) of $CsH_2PO_4(s,pe)$ and the partial pressure of water (p_{H_2O}/atm) is expressed by

$$\log p_{H_2O} = 7.62(\pm 1.18) - 4.42(\pm 0.56)\frac{1000}{T_{dehy}}$$

The stable phase just above T_{dehy} is the fully dehydrated product of solid $CsPO_3$. However, partially dehydrated products, such as solid $CsHPO_{3.5}$ and an unknown phase, appeared as transient phases in the course to complete dehydration. The dehydration mechanism from $CsH_2PO_4(s,pe)$ was explained by thermodynamic considerations. The findings in this study allowed us to complete the temperature-humidity phase diagram of CsH_2PO_4, which is important information for its stable operation as a fuel cell electrolyte. Moreover, the composition-temperature phase diagram of the CsH_2PO_4–$CsPO_3$ system was estimated to be of the eutectic type with no intermediate compound of solid.

The final dehydration product of $CsPO_3$ showed relatively high electrical conductivity in unhumidified Ar. In the intermediate temperature range from 150 to 450°C, $CsPO_3$ exhibited ionic conductivity as high as 5×10^{-4} S cm^{-1} with a property to disappear after first heating. This high ionic conductivity was probably caused by the proton diffusion through the absorbed H_2O on the surface and interface. At ~600°C, after the transition to the high-temperature phase, $CsPO_3$ exhibited high conductivity of $\sim 10^{-3}$ S cm^{-1}. This conductivity was not pure ionic and did not change by heating/cooling cycles.

Acknowledgments

This work was financially supported by Superprotonic, Inc. (California, USA). The authors thank Professor Sossina M. Haile and Ayako Ikeda (California Institute of Technology) for useful discussions.

Kyoto University assisted in meeting the publication costs of this article.

References

1. A. I. Baranov, V. P. Khiznichenko, V. A. Sandler, and L. A. Shuvalov, *Ferroelectrics*, **81**, 1147 (1988).
2. W. Bronowska, *J. Chem. Phys.*, **114**, 611 (2001).
3. J. Otomo, N. Minagawa, C. Wen, K. Eguchi, and H. Takahashi, *Solid State Ionics*, **156**, 357 (2003).
4. D. A. Boysen, S. M. Haile, H. Liu, and R. A. Secco, *Chem. Mater.*, **15**, 727 (2003).
5. S. M. Haile, C. R. I. Chisholm, D. A. Boysen, K. Sasaki, and T. Uda, *Faraday Discuss.*, **17**, 134 (2007).
6. D. A. Boysen, T. Uda, C. R. I. Chisholm, and S. M. Haile, *Science*, **303**, 68 (2004).
7. J. Otomo, T. Tamaki, S. Nishida, S. Wang, M. Ogura, T. Kobayashi, C.-J. Wen, H. Nagamoto, and H. Takahashi, *J. Appl. Electrochem.*, **35**, 865 (2005).
8. T. Uda and S. M. Haile, *Electrochem. Solid-State Lett.*, **8**, A245 (2005).
9. T. Uda, D. A. Boysen, C. R. I. Chisholm, and S. M. Haile, *Electrochem. Solid-State Lett.*, **9**, A261 (2006).
10. Y. Taninouchi, T. Uda, Y. Awakura, A. Ikeda, and S. M. Haile, *J. Mater. Chem.*, **17**, 3182 (2007).
11. Y. Taninouchi, T. Uda, and Y. Awakura, *Solid State Ionics*, **178**, 1648 (2008).
12. D. A. Boysen, Ph.D. Thesis, California Institute of Technology, Pasadena, CA (2004).
13. JCPDS file card no. 84-0122, Joint Committee on Powder Diffraction Standards, Swarthmore, PA.
14. JCPDS file card no. 81-1576, Joint Committee on Powder Diffraction Standards, Swarthmore, PA.
15. R. K. Osterheld and M. M. Markowitz, *J. Phys. Chem.*, **60**, 863 (1956).
16. M. T. Averbuch-Pouchot and A. Durif, *Topics in Phosphate Chemistry*, World Scientific, Singapore (1996).
17. D. D. Wagman, W. H. Evans, V. B. Parker, R. H. Schumm, I. Halow, S. M. Bailey, K. L. Churney, and R. L. Nuttall, *J. Phys. Chem. Ref. Data*, **11**, 2 (1982).
18. E. Rapoport, J. B. Clark, and P. W. Richter, *J. Solid State Chem.*, **24**, 423 (1978).
19. S. J. Kiehl and G. H. Wallace, *J. Am. Chem. Soc.*, **49**, 375 (1927).
20. J. E. Huheey, E. A. Keiter, and R. L. Keiter, *Inorganic Chemistry—Principles of Structure and Reactivity*, 4th ed., Harper Collins, New York (1993).
21. R. D. Shannon, *Acta Crystallogr., Sect. A: Cryst. Phys., Diffr., Theor. Gen. Crystallogr.*, **32**, 751 (1976).